Empirical demonstration of CO_2 detection using macroporous silicon photonic crystals as selective thermal emitters

DAVID CARDADOR MAZA,[1,*] DANIEL SEGURA GARCIA,[1] IOANNIS DERIZIOTIS, [1] MOISÉS GARÍN,[2] JORDI LLORCA, [3,*] ANGEL RODRIGUEZ

[1]*Micro i Nanotecnologies, Departament d'Enginyeria Electrònica, Universitat Politècnica de Catalunya, Jordi Girona, 31, 08031, Barcelona, Spain.*
[2] *GR-MECAMAT, Universitat de Vic – Universitat Central de Catalunya, Campus Torre dels Frares, c/ de la Laura 13, 08500 Vic, Spain.*
[3] *Institute of Energy Technologies, Department of Chemical Engineering Barcelona Research Center in Multiscale Science and Engineering, Universitat Politècnica de Catalunya, Av. Eduard Maristany, 10-14, 08019, Barcelona, Spain.*

**Corresponding author: david.cardador@upc.edu*

Received XX Month XXXX; revised XX Month, XXXX; accepted XX Month XXXX; posted XX Month XXXX (Doc. ID XXXXX); published XX Month XXXX

We report CO_2 detection using macroporous silicon photonic crystals as thermal emitters. We demonstrate that the reduction of structural non-homogeneities leads to an improvement of the photonic crystals' emission. High quality narrow emission bands (Q ~ 120) located within the R-branch of carbon dioxide were achieved. Measurements were made using a DTGS photodetector and the photonic crystals, heated to 400ºC, as selective emitters. A gas cell with a CO_2 concentration between 0 ppm and 10,000 ppm was installed in the center. Results show high sensibility and selectivity that could be used in current NDIR devices for improving their features. These results open the door to narrowband emission in mid infrared for spectroscopic gas detection.

http://dx.doi.org/10.1364/OL.99.099999

Selective thermal emission has recently attracted much attention in non-dispersive infrared (NDIR) detection. The goal is to exhibit narrow emission bands in the specific region where gas molecules or chemical compounds exhibit their vibrational modes [1]. The narrower this band, the more selective and sensitive the detection will be. Currently there are ultra-high resolution laser emitters working in the mid-infrared (MIR) region [2,3]. However, they are very expensive because, among others, a temperature regulation system is needed to avoid displacements of their monochromatic light. On the other hand, there are broadband emitters which rely on metal or semiconductor technology. A commercialized option are mid-IR-LEDs [4,5]. One of the principal problems this technology faces is low output power. Their common values, in the range of few μW, suppose an important restriction to different applications. An alternative to them are thermal emitters, which are based on blackbody radiation. Planck's law states that all bodies above absolute zero transfer energy to the rest of the universe covering all ranges of the electromagnetic spectrum. Conventional NDIR devices employ blackbody thermal sources combined to filters to detect in the species absorption range [1,6]. However, as Miyazaki et al. highlight in [7], NDIR detection is fundamentally an inefficient technique because sensing in a small portion of the spectrum makes most of the radiation being wasted. In the work they use a nanostructured material as a selective thermal emitter for NDIR detection of CO_2. They show a 30% reduction in energy consumption compared to conventional blackbody emitters. However, they do not seek selectivity or improved sensitivity, the main objectives of our work.

One of the most extensively explored solutions for narrowband emitters are photonic crystals (PhCs) due to their ability to control the density of states [8–10]. Different strategies based on plasmon resonances [11] or multi-quantum-well structures [12–14] have proved high-quality emissivity when combined to PhCs. Furthermore, some of them have experimentally demonstrated the feasibility of generating narrow emission bands in the long-infrared fingerprint region of organic solvents and gases [13].

Previous studies reported that 2D-structured bulk silicon increased the surface roughness and therefore higher emittance could be achieved [15]. Others showed the potential application of 3D macroporous silicon PhCs as selective emitters in the absorption regions of CO and NO_2 [16]. The aim of this letter is to enhance the quality of the in-band radiation and demonstrate the viability of gas detection using 3D macroporous silicon photonic crystals.

The structure of the document is as follows. We first show the negative impact that non-homogeneities have in the emission quality of our samples. Next, some modifications are introduced in

the manufacturing process and in the design of the photonic crystals to obtain narrow band emitters located in the carbon dioxide fingerprint. We describe the dispersive detection of CO_2, giving the relationship between the expected power reaching the detector and the concentration of the gas. We finish by showing a proof of concept of the benefits that our emitters would give in terms of sensitivity and selectivity to conventional NDIR devices.

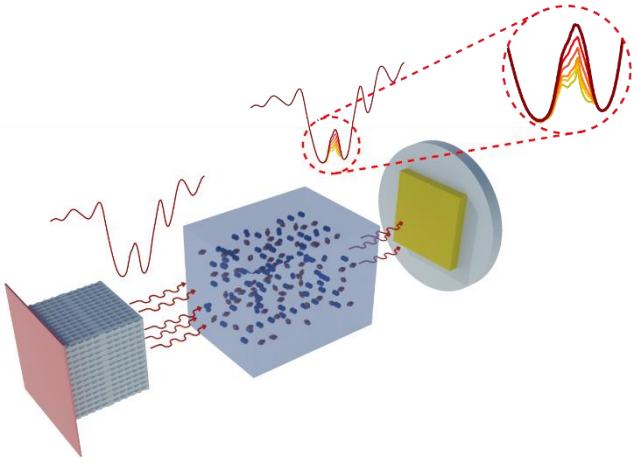

Fig. 1. Schematic of the CO_2 detection process using macroporous silicon photonic crystals as selective emitters; the PhC is heated up to 400 ºC radiating in the MIR with the resonance peak centered in CO_2 absorption range. The electromagnetic field crosses the gas chamber and its concentration is determined by quantifying the difference between the initial and the final emission intensity arriving the detector.

Let us start by introducing the optical response of previously reported samples that showed very low-quality thermal emission [16]. These samples were made through a 5% HF electrochemical etching at 10 ºC, with a constant polarization of 2V and an asymmetric trapezoidal current profile. As a result of the fabrication process, 700 nm pitch PhCs consisting on two modulation areas, with five periods each, and a cavity in the middle were obtained. The total length of the PhCs was around 25 µm and the substrate depth around 250 µm (further details can be found elsewhere [17]).

It is well known that these structures raise resonant modes, or transmitted peaks, within the bandgap due to the cavity inserted in the middle of the modulated regions [17]. Figure 2a depicts the dispersion of the peak along the attacked area. It can be seen that the central frequency, the transmittance, and the quality factor of the peak depends on the selected spot, as suggested in previous studies [18,19]. In other words, we demonstrated the existence of a high number of cooperative resonators along the emitting area, which is around 1 cm^2. Figure 2b shows the average transmittance, T, and reflectance, R, along the area. We can use them to calculate the emissivity, E, of the sample through Kirchhoff's Law, which states that

$$E = 1 - R - T \qquad (1)$$

Figure 2c shows a good agreement between calculated and experimental emissivity, which has been extracted from previous studies [20]. In addition, the shape of both curves have a great similarity with the average transmission of Figure 2b. This confirms that there is a direct relationship between the dispersion, due to structural non-homogeneities of the photonic crystal, and quality of the emission peak.

Based on the above, we set out to improve our fabrication set-up in order to reduce non-homogeneities and thereby increase the quality of emissions. In particular, the uniformity of lighting during the electrochemical process was identified as a key factor; it was observed that samples presented lower quality factors and lower transmissions at the edges than in the center. Therefore, an optical diffuser was included to disperse light and thus improve uniformity. Subsequent measurements revealed a more homogenous response across the emission area. This allowed us to enhance the Q-factor of the structures by increasing the number of periods of the photonic crystals up to eight and ten periods, following the same idea as previous studies [21,22]. As a result of the improvements, the dispersion in 8 and 10 periods was substantially reduced –see Figures 2d and 2g–. Consequently, narrower average transmission peaks were obtained –Figures 2e and 3h.

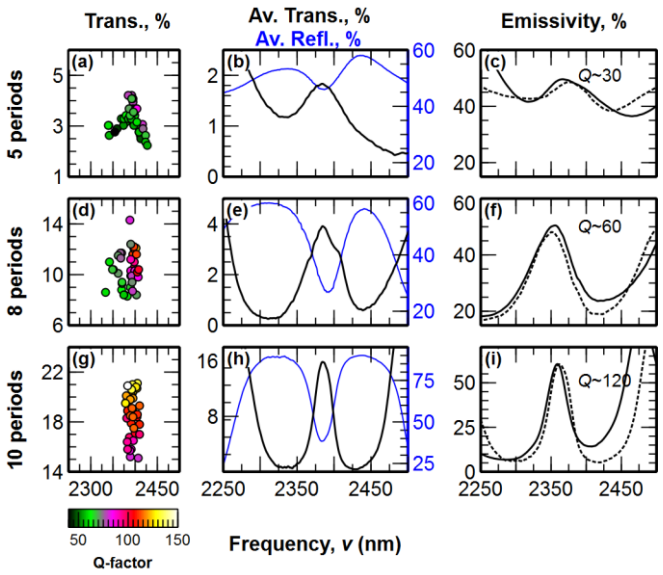

Fig. 2. Dispersion, average transmittance and reflectance, and emissivity for 5, 8 and 10 periods. (Left-column) Colored circles represent the multiple peaks measured along the sample. Their *x*-value is the central frequency and the *y*-value, the transmittance. The color represents the Q-factor. (Middle-column) Average transmittance (black) and reflectance (blue) for all peaks from left column. (Right-column) Emission spectrum of each sample.

We measured photonic crystals' emissivity using a Vertex 70 FT-IR spectrometer equipped with the A540 emission adapter. We heated the samples to 400 ºC and referenced their spectrum to blackbody radiation, which was obtained by heating a carbonized piece of silicon at 400 ºC. Figures 2f and 2i show that emission is improved as we increase the number of periods. On one hand, we can see that the base of the peak is reduced from the initial value of 40% in the case of 5 periods, to 20% and 7% for 8 and 10 periods, respectively. This is due to the fact that light is more filtered as more periods are in the structure. Thus, the amplitude of the peak is increased from 20% to 40% and 55%. For the same reason, the base of the peak is tightened as more periods are added. In Figure 2c we see that the base is 150 cm^{-1} wide while in Figure 2i it has been reduced to 100 cm^{-1}. As a result of both improvements, amplitude enhancement and base narrowing, the quality factor of the peaks doubled and quadrupled the initial value of 30 for 8 and 10 periods, respectively. In addition, we can see that the experimental emissivity is very similar to the calculated using Kirchhoff's Law.

There is another interesting information in the emissivity figures; we can estimate the in-band radiance of our samples, i.e. the emitted power of our peaks, throughout the Planck's Law,

$$\Delta P = A \int_{\upsilon_1}^{\upsilon_2} B_\upsilon = A \frac{2h\upsilon^3}{c^2} \int_{\upsilon_1}^{\upsilon_2} \frac{d\upsilon}{e^{h\upsilon/k_B T}-1} \qquad (2)$$

which describes the radiated power of a black-body, ΔP (W), at a temperature T (K), within a frequency range [ν_1, ν_2] (cm^{-1}), and with an active area A (cm^2). To facilitate it, we numerically computed the integral of the spectral radiance as described by Widger and Woodall [23]. Thus, after setting the appropriate values, T = 400 ºC, A = 1 cm^2, ν_1 = 2300 and ν_2 = 2400 (for 10 period's peak), we got a radiated power of $\Delta P \sim 5$ mW. Note that this value is for a black body. In our case, our maximum emissivity is 62% and the total area of the peak represents the 40% of the blackbody emission within the frequency range, ν_2- ν_1. Therefore, the estimated value of our peak without CO_2 and at 400 ºC is about 2 mW.

Emission peaks for 8 and 10 periods completely fitted into the carbon dioxide fingerprint. This allowed us to perform spectroscopic measurements with the photonic crystals as thermal emitters. For this purpose, we used a DTGS detector from Bruker v-70 FT-IR working in the MIR. We placed a specifically fabricated gas cell of 1.4 cm depth in the middle of the optical path and we introduced CO_2 concentrations ranging from 0 ppm to 10,000 ppm. Next, we measured the variation of the peak area, in essence, the estimated power reaching the receiver, versus the concentration.

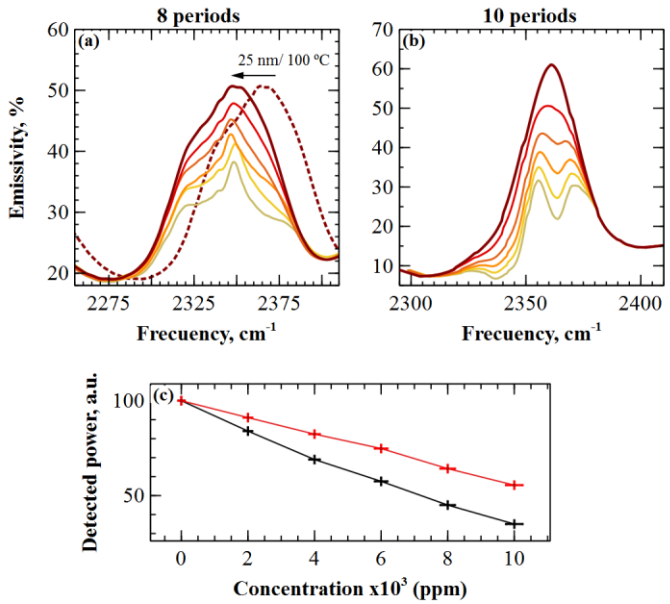

Fig. 3. Emission spectra for 8, a), and 10, b), periods when exposed to 0; 2,000; 4,000; 6,000; 8,000 and 10,000 ppm of CO_2 at 400 ºC. In a), the dotted line indicates the emission spectra at 300 ºC without gas. c) Relationship between the area of the peaks and the concentration (8 periods red line, 10 periods black line).

Figures 3a and 3b depict the optical response of the selective emitters for 8 and 10 periods when exposed to CO_2. We see that, for the same concentrations –i.e. curves with the same color–, the response of the narrower emitter is more accused than for the wider. This is because the peak for 10 periods is comprised within the R branch instead of encompassing the entire absorption range of CO_2, as happens for the 8 period's case. In addition, in Figure 3a we can see that the central frequency of the emission can be precisely tuned by controlling the temperature. In that manner, the position of the peak can be regulated to achieve the most optimal response.

For a more visual interpretation of the results, we plotted the sensitivity curves for 8 and 10 periods in Figure 3c. In essence, each red point corresponds to the normalized area of each one of the peaks in Figure 3a, and the same applies to black points and Figure 3b. Comparing both curves, we see a higher slope for the case of 10 periods, meaning a higher selectivity than for 8 periods. In both measurements the uncertainty in the concentration, given by the error associated in the mass flowmeter, varies from ±100 ppm (lowest concentration) to ±250 ppm (highest concentration).

Up to this point it has been demonstrated that macroporous silicon photonic crystals can be used as selective emitters for CO_2 detection. Let us finish by showing a proof of concept of the benefits that our emitters would bring to current NDIR devices.

NDIR gas sensors [24,25] work with a broadband emitter and a thermopile that detect in a wide range –typically from 2 µm to 20 µm–. Hence, they need a bandpass filter to only sense in the specific area of the gas. Figure 4a shows that our emitting peaks are three times narrower than the filters used in previous gas sensors –red dashed line–. It can also be observed that the bandwidth of our emitters ensures that only the signal below the curve of the emission peak is detected. In other words, the rest of the spectrum is blocked by the filter and only our emission peak, pointing to the R-branch of CO_2, will survive. Consequently, higher sensitivity is reported in Figure 4b.

To calculate the response of the NDIR device for the same path length than ours, we computed the Beer-Lambert Law for broadband spectroscopy [26]. This is, we equally discretized both carbon dioxide spectrum, obtained from HITRAN database [27], and filter transmission, and we applied Equation 3.

$$\frac{I(\nu_i)}{I_0(\nu_i)} = \exp(-C\sigma_{CO_2}(\nu_i)L) \qquad (3)$$

where $I_0(\nu_i)$ and $I(\nu_i)$ are the incident and received radiation intensities at frequency ν_i, respectively; $\sigma_{CO2}(\nu_i)$ (cm^2 molecule^{-1}) is the absorption cross section at frequency ν_i; C (molecules m^{-3}) is the concentration of the gas under test; and L is the absorption optical path length (cm).

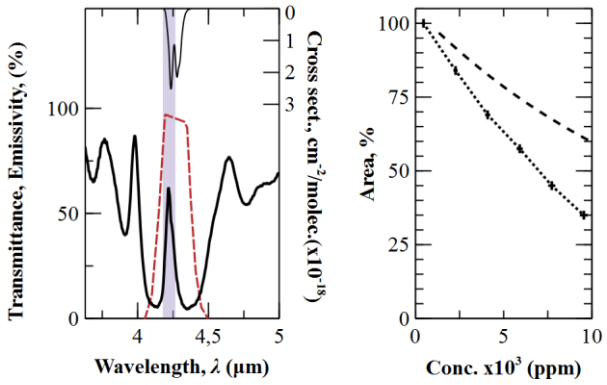

Fig. 4. a) (Left axis) Transmittance of conventional bandpass filters, (dashed red line, data extracted from [24]), emissivity of macroporous silicon PhCs (black) and CO_2 absorption spectrum (grey, right axis). b) PhC (dotted line) and filter (dashed line) selectivity.

The estimated radiated power can be extracted from Equation 1, using same parameters as before except for the emitter area which, in this case is 0.1 cm^2. Therefore, the power in the case without CO_2 would be approximately 200 μW. This value is comparable to the power emitted by the broadband sources used in the device. Further studies should focus on lateral band suppression, e.g. depositing adequate materials in the rear side of the wafer, for filterless detection.

Finally, the authors would like to remark that these results could be used to improve the emissivity reported in previous articles in order to detect CO and NO_2 [20]. Furthermore, thanks to the versatility of the photoelectrochemical etching process, the reported macroporous silicon structures can be designed to specifically work in the entire MIR band. Consequently, these results suppose, not only the evidence of the detection of a specific gas, but the demonstration that this technology can be used to detect other gases in the MIR by optical spectroscopy.

To conclude, in this Letter we have performed corrective actions to improve the emissivity of macroporous silicon photonic crystals; we have reduced the dispersion in the samples and added more periods to the structure. In this manner, we achieved narrowband thermal emitters placed in the carbon dioxide fingerprint. The best case presented an emissivity amplitude of approximately 55% and a q-factor of 120. This allowed spectroscopic detection at the R-branch of CO_2 and its comparison to current NDIR devices. Results show that the use of our emitters would lead to higher sensitivity and selectivity than using broadband sources. In addition, it has been estimated that the emitted power would be very similar to the one radiated using conventional emitters. Finally, we remark that these results can be extended to other gases thus, opening the door to selective emission along the mid-infrared.

Funding. Spanish Ministry of Economy and Competitiveness (MINECO) co-funded by the European Regional Development Fund (TEC-2013-48-147-C6-2, ENE2015-74009-JIN); Spanish Ministry of Science and Innovation/European Regional Development Funds (MICINN/FEDER) (RTI2018-093996-B-C31).

Acknowledgement. JL is a Serra Húnter Fellow and is grateful to ICREA Academia program and GC 2017 SGR 128.

REFERENCES

1. J. Hodgkinson and R. P. Tatam, Meas. Sci. Technol. **24**, 012004 (2013).
2. G. Villares, A. Hugi, S. Blaser, and J. Faist, Nat. Commun. **5**, 5192 (2014).
3. R. Szedlak, A. Harrer, M. Holzbauer, B. Schwarz, J. P. Waclawek, D. MacFarland, T. Zederbauer, H. Detz, A. M. Andrews, W. Schrenk, B. Lendl, and G. Strasser, ACS Photonics **3**, 1794 (2016).
4. M. Aziz, C. Xie, V. Pusino, A. Khalid, M. Steer, I. G. Thayne, and D. R. S. Cumming, Appl. Phys. Lett. **111**, 102102 (2017).
5. LED Microsensor NT, *Mid-Infrared (MIR) Light-Emitting Diode, Lms43LED-RW* (2017).
6. C. Calaza, L. Fonseca, M. Moreno, S. Marco, C. Cané, and I. Gracia, Sensors Actuators A Phys. **113**, 39 (2004).
7. H. T. Miyazaki, T. Kasaya, M. Iwanaga, B. Choi, Y. Sugimoto, and K. Sakoda, Appl. Phys. Lett. **105**, 121107 (2014).
8. S.-Y. Lin, J. G. Fleming, E. Chow, J. Bur, K. K. Choi, and A. Goldberg, Phys. Rev. B **62**, R2243 (2000).
9. A. Narayanaswamy and G. Chen, Phys. Rev. B **70**, 125101 (2004).
10. I. Celanovic, D. Perreault, and J. Kassakian, Phys. Rev. B **72**, 075127 (2005).
11. Z. Wang, J. K. Clark, Y.-L. Ho, B. Vilquin, H. Daiguji, and J.-J. Delaunay, ACS Photonics **5**, 2446 (2018).
12. M. De Zoysa, T. Asano, K. Mochizuki, A. Oskooi, T. Inoue, and S. Noda, Nat. Photonics **6**, 535 (2012).
13. T. Inoue, M. De Zoysa, T. Asano, and S. Noda, Appl. Phys. Lett. **102**, 191110 (2013).
14. T. Inoue, M. De Zoysa, T. Asano, and S. Noda, Nat. Mater. **13**, 928 (2014).
15. W. Konz, J. Hildenbrand, M. Bauersfeld, S. Hartwig, A. Lambrecht, V. Lehmann, and J. Wollenstein, in *Smart Sensors, Actuators, MEMS II. Vol. 5836. Int. Soc. Opt. Photonics*, edited by C. Cane, J.-C. Chiao, and F. Vidal Verdu (International Society for Optics and Photonics, 2005), pp. 540–548.
16. D. Cardador, D. Segura, D. Vega, and A. Rodríguez, in *Proc. 5th Int. Conf. Photonics, Opt. Laser Technol.* (SCITEPRESS - Science and Technology Publications, 2017), pp. 191–195.
17. D. Cardador, D. Vega, D. Segura, and A. Rodríguez, Infrared Phys. Technol. **80**, (2017).
18. S. Matthias, R. Hillebrand, F. Müller, and U. Gösele, J. Appl. Phys. **99**, 113102 (2006).
19. D. Segura, D. Vega, D. Cardador, and A. Rodriguez, Sensors Actuators, A Phys. **264**, (2017).
20. D. Cardador, D. Segura, D. Vega, and A. Rodríguez, in *PHOTOPTICS 2017 - Proc. 5th Int. Conf. Photonics, Opt. Laser Technol.* (2017), pp. 191–194.
21. D. Cardador, D. Vega, D. Segura, T. Trifonov, and A. Rodríguez, Photonics Nanostructures - Fundam. Appl. **25**, 46 (2017).
22. D. Cardador, D. Segura, and A. Rodríguez, Opt. Express **26**, 4621 (2018).
23. W. K. Widger, M. P. Woodall, J. W. K. Widger, and M. P. Woodall, Bull. Am. Meteorol. Soc. **57**, 1217 (1976).
24. J. Hodgkinson, R. Smith, W. O. Ho, J. R. Saffell, and R. P. Tatam, Sensors Actuators B Chem. **186**, 580 (2013).
25. R. Lee and W. Kester, *Complete Gas Sensor Circuit Using Nondispersive Infrared (NDIR)* (2016).
26. H. S. Wang, Y. G. Zhang, S. H. Wu, X. T. Lou, Z. G. Zhang, and Y. K. Qin, Appl. Phys. B **100**, 637 (2010).
27. S. A. Tashkun, V. I. Perevalov, R. R. Gamache, and J. Lamouroux, J. Quant. Spectrosc. Radiat. Transf. **152**, 45 (2015).

REFERENCES

1. J. Hodgkinson and R. P. Tatam, Meas. Sci. Technol. **24**, 012004 (2013).
2. G. Villares, A. Hugi, S. Blaser, and J. Faist, Nat. Commun. **5**, 5192 (2014).
3. R. Szedlak, A. Harrer, M. Holzbauer, B. Schwarz, J. P. Waclawek, D. MacFarland, T. Zederbauer, H. Detz, A. M. Andrews, W. Schrenk, B. Lendl, and G. Strasser, ACS Photonics **3**, 1794 (2016).
4. M. Aziz, C. Xie, V. Pusino, A. Khalid, M. Steer, I. G. Thayne, and D. R. S. Cumming, Appl. Phys. Lett. **111**, 102102 (2017).
5. LED Microsensor NT, *Mid-Infrared (MIR) Light-Emitting Diode, Lms43LED-RW* (2017).
6. C. Calaza, L. Fonseca, M. Moreno, S. Marco, C. Cané, and I. Gracia, Sensors Actuators A Phys. **113**, 39 (2004).
7. H. T. Miyazaki, T. Kasaya, M. Iwanaga, B. Choi, Y. Sugimoto, and K. Sakoda, Appl. Phys. Lett. **105**, 121107 (2014).
8. S.-Y. Lin, J. G. Fleming, E. Chow, J. Bur, K. K. Choi, and A. Goldberg, Phys. Rev. B **62**, R2243 (2000).
9. A. Narayanaswamy and G. Chen, Phys. Rev. B **70**, 125101 (2004).
10. I. Celanovic, D. Perreault, and J. Kassakian, Phys. Rev. B **72**, 075127 (2005).
11. Z. Wang, J. K. Clark, Y.-L. Ho, B. Vilquin, H. Daiguji, and J.-J. Delaunay, ACS Photonics **5**, 2446 (2018).
12. M. De Zoysa, T. Asano, K. Mochizuki, A. Oskooi, T. Inoue, and S. Noda, Nat. Photonics **6**, 535 (2012).
13. T. Inoue, M. De Zoysa, T. Asano, and S. Noda, Appl. Phys. Lett. **102**, 191110 (2013).
14. T. Inoue, M. De Zoysa, T. Asano, and S. Noda, Nat. Mater. **13**, 928 (2014).
15. W. Konz, J. Hildenbrand, M. Bauersfeld, S. Hartwig, A. Lambrecht, V. Lehmann, and J. Wollenstein, in *Smart Sensors, Actuators, MEMS II. Vol. 5836. Int. Soc. Opt. Photonics*, edited by C. Cane, J.-C. Chiao, and F. Vidal Verdu (International Society for Optics and Photonics, 2005), pp. 540–548.
16. D. Cardador, D. Segura, D. Vega, and A. Rodríguez, in *Proc. 5th Int. Conf. Photonics, Opt. Laser Technol.* (SCITEPRESS - Science and Technology Publications, 2017), pp. 191–195.
17. D. Cardador, D. Vega, D. Segura, and A. Rodríguez, Infrared Phys. Technol. **80**, (2017).
18. S. Matthias, R. Hillebrand, F. Müller, and U. Gösele, J. Appl. Phys. **99**, 113102 (2006).
19. D. Segura, D. Vega, D. Cardador, and A. Rodriguez, Sensors Actuators, A Phys. **264**, (2017).
20. D. Cardador, D. Segura, D. Vega, and A. Rodríguez, in *PHOTOPTICS 2017 - Proc. 5th Int. Conf. Photonics, Opt. Laser Technol.* (2017), pp. 191–194.
21. D. Cardador, D. Vega, D. Segura, T. Trifonov, and A. Rodríguez, Photonics Nanostructures - Fundam. Appl. **25**, 46 (2017).
22. D. Cardador, D. Segura, and A. Rodríguez, Opt. Express **26**, 4621 (2018).
23. W. K. Widger, M. P. Woodall, J. W. K. Widger, and M. P. Woodall, Bull. Am. Meteorol. Soc. **57**, 1217 (1976).
24. J. Hodgkinson, R. Smith, W. O. Ho, J. R. Saffell, and R. P. Tatam, Sensors Actuators B Chem. **186**, 580 (2013).
25. R. Lee and W. Kester, *Complete Gas Sensor Circuit Using Nondispersive Infrared (NDIR)* (2016).
26. H. S. Wang, Y. G. Zhang, S. H. Wu, X. T. Lou, Z. G. Zhang, and Y. K. Qin, Appl. Phys. B **100**, 637 (2010).
27. S. A. Tashkun, V. I. Perevalov, R. R. Gamache, and J. Lamouroux, J. Quant. Spectrosc. Radiat. Transf. **152**, 45 (2015).